Motile cilia of the male reproductive system require miR-34/miR-449 for development and function to generate luminal turbulence

Shuiqiao Yuan[a,b,1], Yue Liu[c,d,1], Hongying Peng[a,1], Chong Tang[a], Grant W. Hennig[a,e], Zhuqing Wang[a], Li Wang[c,d], Tian Yu[a], Rachel Klukovich[a], Ying Zhang[a], Huili Zheng[a], Chen Xu[c,d,2], Jingwen Wu[c,d,2], Rex A. Hess[f,2], and Wei Yan[a,g,2]

[a]Department of Physiology and Cell Biology, University of Nevada, Reno School of Medicine, Reno, NV 89557; [b]Family Planning Research Institute, Center for Reproductive Medicine, Tongji Medical College, Huazhong University of Science and Technology, 430030 Wuhan, China; [c]Department of Histology, Embryology and Genetics, Shanghai Jiaotong University School of Medicine, 200025 Shanghai, China; [d]Shanghai Key Laboratory of Reproductive Medicine, 200025 Shanghai, China; [e]Department of Pharmacology, University of Vermont, Burlington, VT 05405; [f]Department of Comparative Biosciences, College of Veterinary Medicine, University of Illinois, Urbana, IL 61802; and [g]Department of Obstetrics and Gynecology, University of Nevada, Reno School of Medicine, Reno, NV 89557

Edited by R. Michael Roberts, University of Missouri-Columbia, Columbia, MO, and approved December 14, 2018 (received for review October 3, 2018)

Cilia are cell-surface, microtubule-based organelles that project into extracellular space. Motile cilia are conserved throughout eukaryotes, and their beat induces the flow of fluid, relative to cell surfaces. In mammals, the coordinated beat of motile cilia provides highly specialized functions associated with the movement of luminal contents, as seen with metachronal waves transporting mucus in the respiratory tract. Motile cilia are also present in the male and female reproductive tracts. In the female, wave-like motions of oviductal cilia transport oocytes and embryos toward the uterus. A similar function has been assumed for motile cilia in efferent ductules of the male—i.e., to transport immotile sperm from rete testis into the epididymis. However, we report here that efferent ductal cilia in the male do not display a uniform wave-like beat to transport sperm solely in one direction, but rather exert a centripetal force on luminal fluids through whip-like beating with continual changes in direction, generating turbulence, which maintains immotile spermatozoa in suspension within the lumen. Genetic ablation of two miRNA clusters (*miR-34b/c* and *-449a/b/c*) led to failure in multiciliogenesis in murine efferent ductules due to dysregulation of numerous genes, and this mouse model allowed us to demonstrate that loss of efferent duct motile cilia causes sperm aggregation and agglutination, luminal obstruction, and sperm granulomas, which, in turn, induce back-pressure atrophy of the testis and ultimately male infertility.

multiciliogenesis | male infertility | fluid resorption | reproductive tract | microRNA

Multiciliated cells populate the epithelium of specific mammalian organs. Defects in motile and nonmotile ciliary structures lead to numerous diseases that were first called the immotile cilia syndrome and are now generally labeled as ciliopathies (1–3). The coordinated beat of these cellular appendages induces the flow of fluid over cell surfaces—e.g., in trachea, the metachronal wave of cilial beating transports mucus and trapped debris out of the respiratory system (4). The beating of ependymal cell cilia, in brain ventricles and the spinal column, ensures the movement of spinal fluid (5). Motile cilia are present also in the male and female reproductive tracts. In the female, wave-like motions of oviductal cilia transport oocytes and embryos along the lumen toward the uterus, where implantation occurs (6). In the male, a small tubular organ called efferent ductules (EDs) also possesses motile cilia (7). These ductules convey spermatozoa from rete testis to the caput epididymis, where sperm undergo further maturation to gain fertilizing capability (8). Spermatozoa are immotile and suspended in an abundance of seminiferous tubular fluid when they leave the testis. Before reaching the caput epididymis, nearly 95% of this fluid must be reabsorbed to increase the concentration of luminal spermatozoa. Reabsorption of the fluid is accomplished primarily by the nonciliated cells of the ED epithelium (9). Therefore, for many years, it was assumed—and today is still widely promoted—that the beat of cilia participates in the physical movement of spermatozoa into the epididymis (10–12). Such a function would be similar to ciliary function in the female reproductive system. However, direct measurements of ciliary beat activity in EDs have not been reported.

We and others recently discovered that simultaneous genetic ablation of two microRNA clusters, *miR-34b/c* and *-449a/b/c*, in mice (miR-dKO) inhibited the formation of motile cilia in multiciliated epithelia (13–15). The miR-dKO mice generally display neonatal lethality; however, those that manage to survive later demonstrate infertility, brain abnormalities, and respiratory tract obstructions (14). Early studies of this animal model have suggested that male infertility may result from spermatogenic

Significance

Motile cilia are found lining the respiratory and reproductive systems, as well as the brain and spinal column, and the coordinated beat moves fluids over the luminal surfaces. Disruptions of ciliary structure or beat patterns have been shown to be involved in numerous diseases called ciliopathies. For many years, it has been proposed that the ciliary beat in the male reproductive system propels sperm from testis into the epididymis via tiny efferent ductules. Here, we show that motile cilia lining the efferent ductules do not directly propel sperm, but rather serve as agitators, generating vigorous fluidic turbulence, to maintain suspension of sperm within the intraluminal fluid, thus ensuring an equilibrium in fluid reabsorption by the nonciliated cells.

Author contributions: C.X., J.W., R.A.H., and W.Y. designed research; S.Y., Y.L., H.P., C.T., G.W.H., Z.W., L.W., T.Y., R.K., Y.Z., H.Z., J.W., and W.Y. performed research; S.Y., Y.L., H.P., C.T., G.W.H., Z.W., L.W., C.X., J.W., R.A.H., and W.Y. analyzed data; and R.A.H. and W.Y. wrote the paper.

The authors declare no conflict of interest.

This article is a PNAS Direct Submission.

Data deposition: The RNA-seq data have been deposited into the National Center for Biotechnology Information Sequence Read Achieve database (accession no. PRJNA454757).

See Commentary on page 3361.

[1]S.Y., Y.L., and H.P. contributed equally to this work.

[2]To whom correspondence may be addressed. Email: chenx@shsmu.edu.cn, zpwujw@shsmu.edu.cn, rexhess@illinois.edu, or wyan@med.unr.edu.

This article contains supporting information online at www.pnas.org/lookup/suppl/doi:10.1073/pnas.1817018116/-/DCSupplemental.

Published online January 18, 2019.

disruptions in the testis (14, 15). However, the unique testicular histology in these miR-dKO male mice, characterized by enlarged seminiferous tubule lumens and reduced stratification of the seminiferous epithelium containing a significantly reduced number of spermatogenic cells, has also been observed in mice with disrupted EDs after exposure to environmental chemicals and loss of estrogen receptor-α (ESR1) (16, 17). Therefore, it is highly likely that disrupted multiciliogenesis in the EDs of the miR-dKO mice could be the primary cause of male infertility. To test this hypothesis, we generated spermatogenic cell-specific and multiciliated cell-specific double miRNA cluster knockout mice and also conducted a thorough investigation of ciliary development and the beat patterns observed in ED epithelia and determined the impact of kinetic cilia on the luminal contents.

Results

Inactivation of *miR-34b/C* and *-449* Causes Aberrant Multiciliogenesis, Leading to ED Obstructions, Spermatogenic Disruptions, and Male Infertility. We have previously shown that inactivation of two miRNA clusters, *miR-34b/c* and *-449*, leads to male infertility due to severe depletion of spermatogenic cells within the seminiferous epithelium (14). To test whether defects in spermatogenic cells are the primary cause of male infertility, a spermatogenic cell-specific, *miR-34b/c–miR-449* double conditional knockout mouse line was generated by using *Stra8-Cre* mice as the deletor line (18) (herein called Stra8-miR-dcKO; *SI Appendix*, Fig. S1*A*). Interestingly, the Stra8-miR-dcKO males displayed normal spermatogenesis (*SI Appendix*, Fig. S1*B*) and were completely fertile, suggesting that the phenotype observed in the miR-dKO males does not result from defects in spermatogenic cells. Both the increased testis weight and enlarged lumen of the seminiferous tubules in miR-dKO males (14, 15), however, suggested that there was fluid retention, indicative of potential obstructions in the reproductive tract (16, 19). By microscopic examination of EDs, we observed sperm agglutinations (asterisks in Fig. 1*A* and *SI Appendix*, Fig. S2) in the lumen of EDs in miR-dKO males starting from 1.5 mo of age (coinciding with the completion of the first spermatogenic cycle) and persisting thereafter (3, 8, and 12 mo), whereas spermatozoa were rarely seen in the lumen of proximal EDs in wild-type (WT) controls (Fig. 1*A*). Large-diameter sperm agglutinations (up to 75 μm) were present in the lumen of proximal EDs at 1.5 mo of age (*SI Appendix*, Fig. S2), suggesting that luminal obstructions in miR-dKO mice had begun during the first wave of testicular spermatozoa. Consistent with sperm agglutination, miR-dKO EDs displayed greater opacity/light absorbance under transillumination light (Fig. 1*B*). The agglutination of spermatozoa into large luminal masses would completely obstruct the distal EDs, because the diameter of the distal ED is ∼50 μm (*SI Appendix*, Fig. S2). Indeed, the enlarged lumen of the seminiferous tubules, indicative of fluid retention, was observed in miR-dkO males as early as 1.5 mo (Fig. 1*C*), and the seminiferous epithelium became increasingly thinner (Fig. 1*C*). At 8 mo of age, in addition to the presence of sperm agglutination, macrophages were observed penetrating the ED epithelium and residing in the lumen (*SI Appendix*, Fig. S2). In regions where spermatozoa were not agglutinated, they displayed coiled tails (*SI Appendix*, Fig. S2), suggesting abnormal ED fluid osmolarity (20). At 10–12 mo of age, large sperm granulomas were observed in the rete testis (Fig. 1*A* and *SI Appendix*, Fig. S2), indicating worsened ED obstructions in miR-dKO EDs. By 16 mo of age, atrophy had become so severe that some seminiferous tubules in the miR-dKO testes displayed a "Sertoli cell-only" appearance (Fig. 1*C*). These findings strongly suggest that spermatogenic disruptions in miR-dKO testes result from fluid retention and back pressure due to ED obstructions by sperm plugs in the distal ductules.

The clogged EDs hinted that structural and/or functional defects were present. Indeed, transmission electron microscopic examination revealed that miR-dKO EDs lacked nearly all cilia in the epithelium (Fig. 1*D*). The nonciliated cells showed fairly normal morphology, although appearing stretched and thinner in areas of luminal dilation. Nonciliated cells of miR-dKO had numerous microvilli, similar to WT ED (Fig. 1*D*). In the WT ED epithelium, long cilia extended into the lumen from the ciliated cells, and their basal bodies were located in a row, parallel to the surface (red arrowheads in Fig. 1 *D*, *Left Lower*). In contrast, very few ciliated cells possessed cilia extending into the lumen in miR-dKO EDs and, when present, appeared much shorter in length (*SI Appendix*, Fig. S2). The miR-dKO cells displayed an accumulation of disorganized centrioles in the apical cytoplasm (red arrowheads in Fig. 1 *D*, *Right Lower*), suggesting an inability to attach to the apical plasmalemma and to establish mature basal bodies, from which to grow the ciliary axonemes. In some areas, the nonciliated cells of miR-dKO had numerous microvilli, similar to WT ED (Fig. 1*D*), but in other areas, microvilli were reduced, suggesting that loss of motile cilia may have had indirect effects on the nonciliated cells.

The five miRNAs encoded by the two miRNA clusters were abundantly expressed in EDs, as demonstrated by both quantitative real-time PCR (qPCR) and in situ hybridization analyses (Fig. 2 *A*–*C*). To demonstrate that it is the cilial defects that cause the ED obstructions, followed by fluid retention and back pressure which, in turn, destroys spermatogenesis in miR-dKO mice, we generated another cell-specific knockout mouse line using *Foxj1-Cre* mice as the deletor (herein called Foxj1-dcKO), which expresses Cre exclusively in multiciliated cells (21). The Foxj1-dcKO males displayed a similar phenotype to that of the global miR-dKO males and the *Villin-cre*;*E2f4*$^{f/f}$;*E2f5*$^{+/-}$ mutants (14, 22), characterized by a lack of cilia in the EDs (Fig. 2*D*) and male infertility due to spermatogenic disruptions caused by fluid back pressure after ED obstructions induced by sperm agglutination (Fig. 2*E*). These results unequivocally demonstrate that the five miRNAs are required for multiciliogenesis in the ED epithelium and also suggest that a lack of motile cilia causes ED obstructions, leading to fluid accumulation and germ-cell depletion in the seminiferous tubules.

Effects of Efferent Ductal Obstructions. If back pressure is the cause of spermatogenic disruptions observed in both miR-dKO and Foxj1-dcKO males, then artificial blockage by ED ligation should recapitulate the phenotype in WT mice (23). Indeed, by ligating the EDs using a surgical thread in WT males for 7 and 15 d, enlarged lumens and reduced stratification of the seminiferous epithelium were observed in the testis (*SI Appendix*, Fig. S3 *A* and *B*), resembling those in miR-dKO and Foxj1-dcKO males (Figs. 1*C* and 2*E*). The phenotype was reversed 30 d after ligature removal (*SI Appendix*, Fig. S3 *A* and *B*), suggesting that ED obstructions indeed cause fluid retention and back pressure, leading to germ-cell depletion in the seminiferous epithelium.

If miR-dKO and Foxj1-dcKO testes contain spermatogonia, especially spermatogonial stem cells, spermatogenesis would recover once back pressure is removed. To this end, two tiny holes were made near the rete testis by using a hooked suture needle (0.6 mm in diameter) to release fluid from the rete testis, which is continuous with the seminiferous tubules. Indeed, spermatogenesis recovered almost fully within 15–30 d after pressure relief in both younger (6- to 7-wk-old and 5- to 7-mo-old) and older (12-mo-old) miR-dKO male mice (Fig. 3 and *SI Appendix*, Figs. S3 *C* and *D* and S4). These data suggest that (*i*) back pressure is indeed the cause of massive spermatogenic cell depletion and male infertility; and (*ii*) male fertility can be regained even after long-term spermatogenic disruptions due to back pressure caused by ED obstructions and fluid retention. Taken together, we have demonstrated here that disrupted spermatogenesis due to ED obstructions can fully recover once back pressure is relieved.

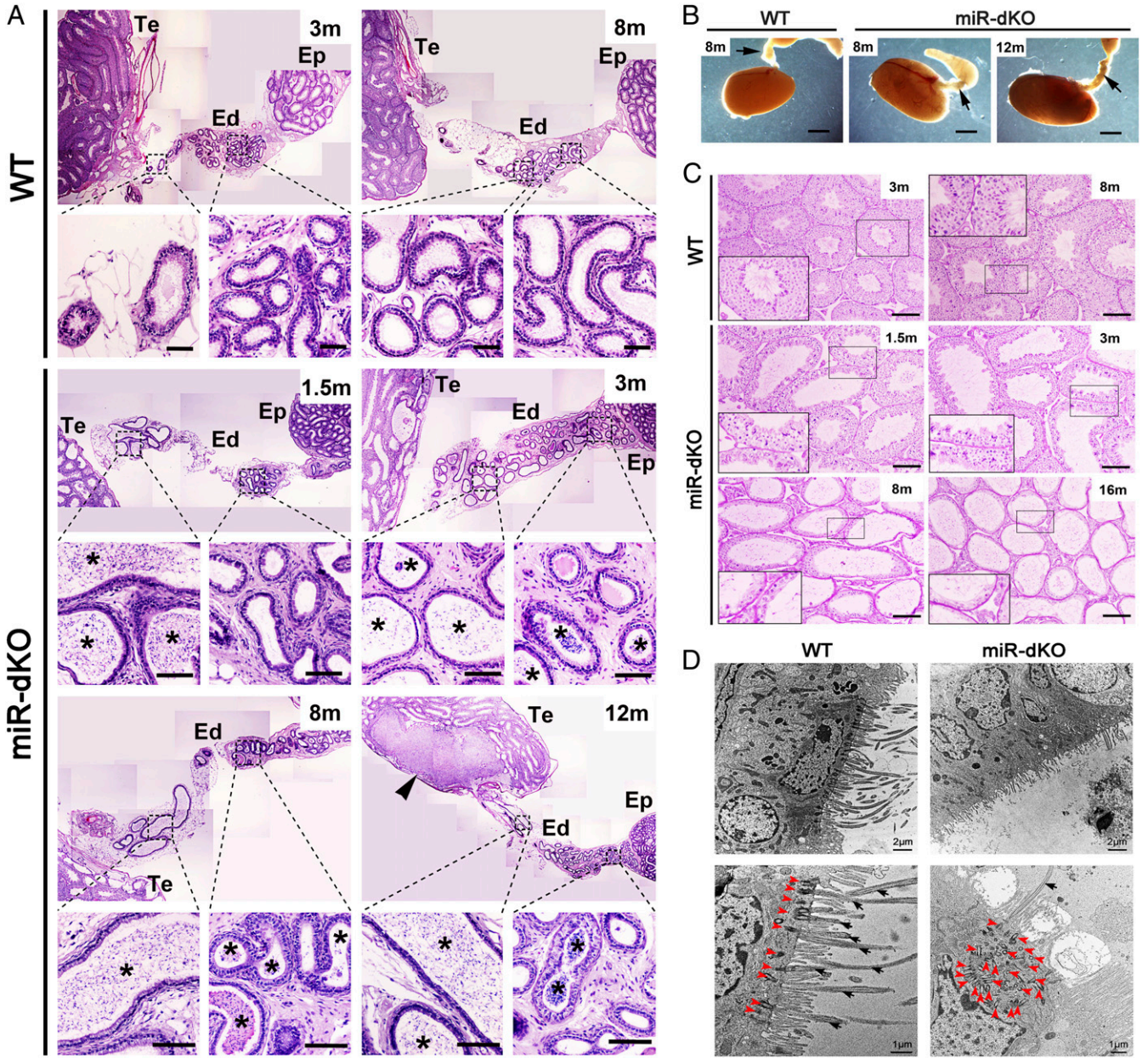

Fig. 1. Spermatogenic disruptions, efferent ductal occlusion, and motile cilial defects in miR-dKO male mice. (*A*) H&E-stained paraffin sections showing that concentrated sperm/sperm agglutinations (asterisks) are present in the lumen of the EDs in miR-dKO males. While spermatozoa are rarely seen in the lumen of WT EDs in the proximal and conus segments, the miR-dKO EDs are filled with high concentrations of spermatozoa, initially only in the proximal segments at 1.5 mo of age, and then spread to the entire length thereafter (3, 8, and 12 mo of age). Sperm granuloma (arrowhead) is obvious in the rete testis of a 12-mo-old miR-dKO male mouse. Ep, epididymis; Te, testis. (Scale bars: 200 μm.) Note: Multiple panels of low-power images were assembled to view the entire EDs. (*B*) Trans-illumination patterns of the EDs in WT (8-mo-old) and miR-dKO (8- and 12-mo-old) mice. Arrows point to the EDs. WT ductules are smaller and nearly translucent, while miR-dKO ductules appear thicker and show more light absorption, indicative of ductules filled with stagnant spermatozoa. (Scale bars: 1 mm.) (*C*) H&E-stained paraffin sections showing that the miR-dKO testes display disrupted spermatogenesis characterized by reduced stratification of seminiferous epithelia and dilated lumens compared with WT testes. The severity of disruptions was increased with age (from 1.5 to 3, 8, and 16 mo). *C*, *Insets* show the digitally amplified subfields (framed). (Scale bars: 200 μm.) (*D*) Transmission electron microscopic images of the epithelium of WT and miR-dKO EDs. In miR-dKO ductules, fewer ciliated cells are observed, and, when present, only rare motile cilia are found extending into the lumen (black arrowheads). However, multiple disorganized centrioles (red arrowheads) are seen in the apical cytoplasm. Nonciliated cells appear normal with microvilli extending into the lumen. WT EDs display fully developed and well-aligned basal bodies along the surface of the ciliated cells, with numerous long motile cilia extending into the lumen.

Ciliated Cells Function as Agitators to Prevent Spermatozoa from Clogging the EDs. Although ciliated cells have been proposed to propel spermatozoa to the epididymis through synchronized beat (24), and preliminary observations have also suggested that ED cilia may function to stir luminal fluid by their "twisting" motions (7, 25), visualization and direct measurements of the beat patterns of ED motile cilia have never been conducted. ED development was first studied and the diameter was found to decrease while the density of ciliated cells increased from proximal to distal segments of EDs during postnatal development (*SI Appendix*, Fig. S5). These results are consistent with those reported in rat EDs (26, 27). Data from the miR-dKO mice strongly

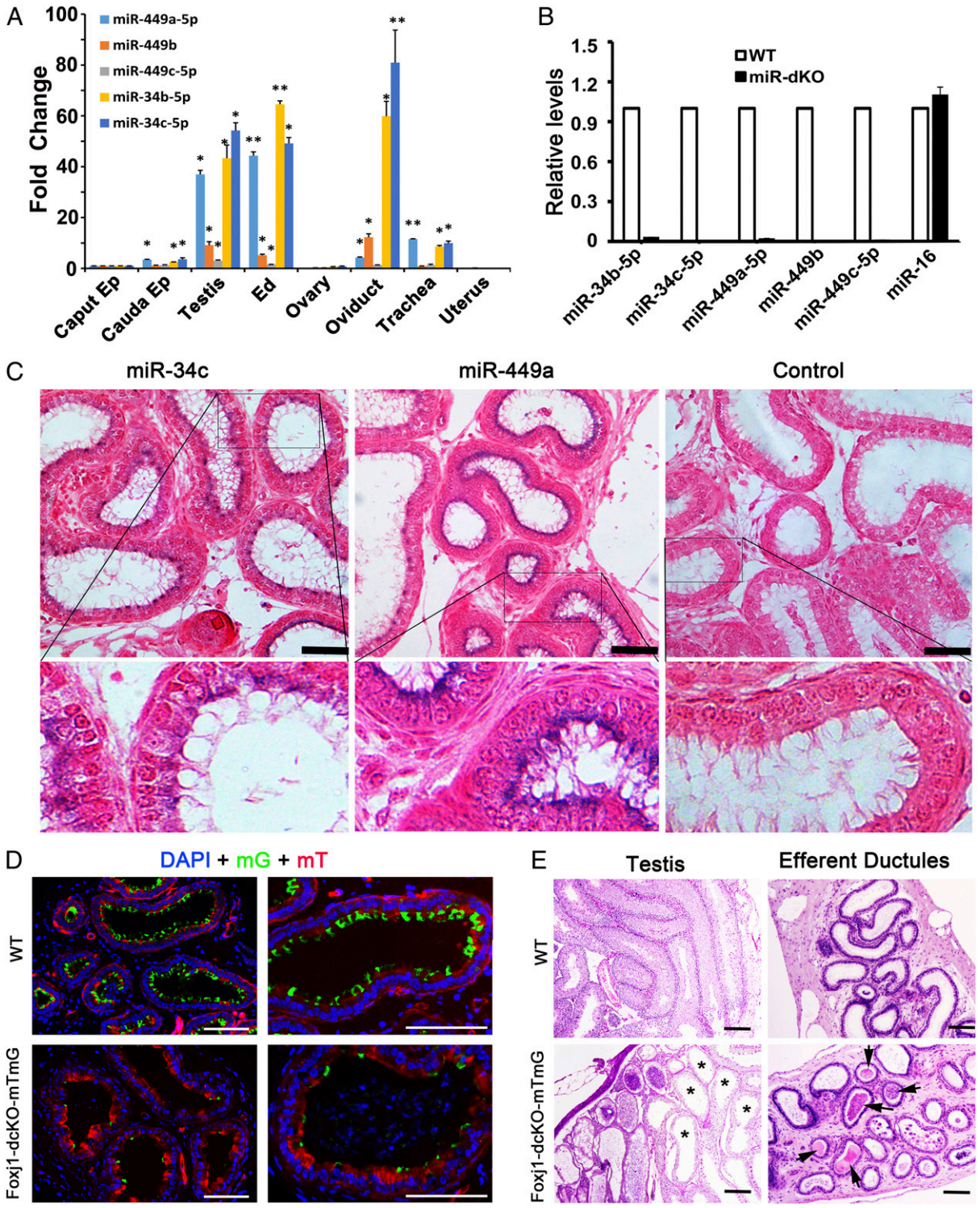

Fig. 2. miR-34b/c and -449a/b/c are abundantly expressed in the ciliated cells of EDs and mice with ciliated cell-specific knockout of the five miRNAs phenocopy the global double miRNA cluster knockout mice. (*A*) qPCR analyses on miR-34b/c and -449a/b/c expression levels in the caput and cauda epididymis (Ep), testis, EDs, ovary, oviduct, trachea, and uterus. U6 snRNA was used as an internal control, and the fold changes were calculated against levels in the caput epididymis. Data are presented as mean ± SEM ($n = 3$). *$P < 0.05$; **$P < 0.01$ (Student t test). (*B*) qPCR analyses on miR-34b/c and -449a/b/c expression levels in WT and miR-dKO EDs. miR-16 was used as an internal control. Data are presented as mean ± SEM ($n = 3$). (*C*) In situ hybridization results showing that both miR-34c and -449a are localized to the ciliated cells in the efferent ductal epithelium. Specific hybridization signals are blue. (Scale bars: 50 μm.) (*D*) Fluorescent microscopic images showing cross-sections of EDs in control (*Foxj1-Cre;Rosa26mTmG*$^{+/Tg}$) and Foxj1-dcKO-mTmG (*Foxj1-Cre;Rosa26mTmG*$^{+/Tg}$*;miR-34b/c*$^{-/-}$*;miR-449*$^{lox/lox}$) mice. Expression of membrane-bound EGFP (mG) is indicative of Cre-expressing ciliated cells. The mG-positive ciliated cells are far fewer in Foxj1-dcKO-mTmG EDs than in controls. (Scale bars: 100 μm.) (*E*) H&E-stained paraffin sections of testes and EDs in WT (*Foxj1-Cre;Rosa26mTmG*$^{+/Tg}$) and Foxj1-dcKO-mTmG (*Foxj1-Cre;Rosa26mTmG*$^{+/Tg}$*;miR-34b/c*$^{-/-}$*;miR-449*$^{lox/lox}$) mice. Ciliated cell-specific conditional knockout (Foxj1-dcKO) males appear to phenocopy the global knockout (miR-dKO) males because both display efferent ductal occlusion and sperm agglutination (arrows), as well as disrupted spermatogenesis due to dilated seminiferous tubules (asterisks). (Scale bars: 100 μm.)

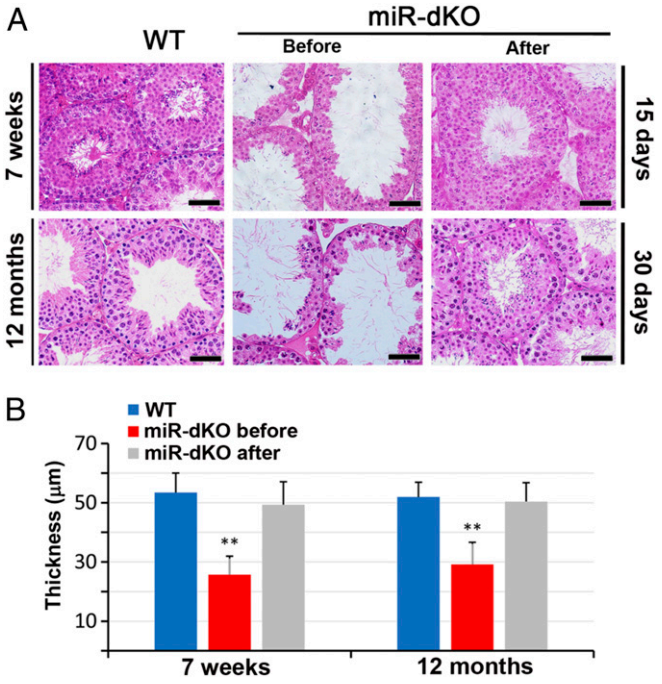

Fig. 3. Testicular histology showing full recovery of spermatogenesis in miR-dKO males after surgical relief of the back pressure. (*A*) Testes of 7-wk-old and 12-mo-old miR-dKO mice showed disrupted spermatogenesis characterized by reduced stratification of seminiferous epithelia and enlarged lumen indicative of back pressure due to fluid retention. By generating two tiny holes using a hooked surgical needle (diameter = 0.6 mm) in the rete testes, the back pressure was released, and full spermatogenesis, similar to that in WT testes, was observed 15 and 30 d after the procedure. (Scale bars: 40 μm.) (*B*) Quantitative analyses of the thickness of seminiferous epithelia in WT and miR-dKO testes before and after the surgical procedure to relieve the back pressure. Data are presented as mean ± SEM ($n = 3$). $^{**}P < 0.01$ (Student *t* test).

indicate that the ED motile cilia can prevent spermatozoa from clogging the ductal lumen. To reveal how motile cilia fulfill this function, the cilial beat patterns and fluid dynamics within the ED lumen were studied through live imaging analyses. Individual ciliated cells isolated from the murine EDs had a unique morphology, consisting of: (*i*) a large, opaque, round cell body (~10.2 ± 1.1 μm in diameter, $n = 6$); (*ii*) a transparent midpiece that appeared to be cylindrical or conical in shape; and (*iii*) a fringe of cilia (~17.5 ± 2.6 μm long, $n = 6$) (Fig. 4*A* and Movies S1 and S2). The movement of cilia on individual ciliated cells was highly uniform and coordinated and appeared as a propagating, waving, or whipping motion of the ciliated fringe (Fig. 4 *A* and *B*). In some instances, a spiraling motion of the elongated cilia was observed, likely due to both side-to-side and up-and-down movements. The coordinated beating motion of isolated ciliated cells caused significant rotational forces applied to the rest of the cell body, with the power stroke rotating the cell body by ~20° and displacing it by ~3–5 μm per beat (Fig. 4*C* and Movies S1 and S2). The distribution of actively beating cilia in intact EDs was visualized by using spatiotemporal (ST) maps (time in the *x* axis) and was often "patchy" (Fig. 4*D* and Movie S3). The frequency and direction of cilial beating were all different among adjacent ciliated cells. Frequencies varied from ~2 to 8 Hz (Fig. 4*E*). The side and top views of an intact ED further revealed the highly variable beating frequencies and directions (Movies S4 and S5). The effects of this variable, multidirectional cilial beating on fluid dynamics could be visualized by the movements of small and large particles within the lumen of the ED (Fig. 4*F* and Movie S3). Smaller particles were propelled at higher velocities in many directions, creating variable trajectories, whereas larger clumps of material were rotated and displaced back and forth over time (swirling motion), displaying spirals in ST objects (Fig. 4*G* and Movie S3). In the miR-dKO EDs, motile cilia were rarely seen and, when observed, were shorter than normal, and the occasional cilial beat was much weaker compared with WT controls (Movie S6). In contrast to the vigorous swirling motion of the contents within WT EDs (Movie S7), almost no motions were observed within the miR-dKO EDs (Movie S8). This explains why immotile testicular spermatozoa, after entering EDs, would precipitate and clog the lumen rapidly in miR-dKO mice. Together, these observations support the notion that motile cilia in the ED epithelium mainly function as agitators, causing vigorous turbulence in all directions so that spermatozoa remain suspended constantly within the ED lumen.

Slow Propagating Contractions of Smooth Muscle Result in Massive Movement of Spermatozoa in the Lumen of EDs. In proximal EDs, spermatozoa were often seen moving in two opposite directions, consistent with the swirling motion of luminal fluid (Movie S9). In distal EDs, rapid ciliary beats were observed to agitate immotile spermatozoa, but these motions appeared to result in minimal forward movement (Movie S10). The propagating contraction of ED smooth muscle narrowed the lumen and pushed spermatozoa rapidly downstream, similar to peristalsis, as shown in a shorter clip at normal playback speed in Movie S10 and a longer clip at faster playback speed in Movie S11. As contractions ended, sperm appeared to flow back into the relaxing segment (Movies S10 and S11). An ST map of wall motion (upper green edge in Fig. 5 *A* and *B*) revealed regular peristaltic contractions that occurred approximately every minute (interval 58.5 ± 4.7 s; $o = 5$) and lasted ~20 s (Fig. 5*C*). ST map analyses of the movement of contents (sperm) within the ED lumen showed that peristaltic contractions of the ED propelled sperm rapidly at velocities of 100–300 $\mu m \cdot s^{-1}$ (Fig. 5 *C–E*). In between peristaltic contractions, sperm movement was variable and slow (10–70 $\mu m \cdot s^{-1}$) (Fig. 5 *C–E*). These observations suggest that cilia-generated movement is local and far less powerful and efficient than smooth muscle contractions in propelling the spermatozoa toward the caput epididymis.

***miR-34b/C* and *miR449* Control Multiciliogenesis by Targeting Key Ciliogenic Genes in the EDs.** To further study how the five miRNAs encoded by the two miRNA clusters regulate multiciliogenesis in EDs, the targets of the five miRNAs were first analyzed by performing RNA deep sequencing (RNA-seq) using miR-dKO and WT EDs (Fig. 6 and *SI Appendix*, Fig. S6). A total of 7,002 genes were identified to be dysregulated, including 3,879 genes up-regulated and the rest (3,123) down-regulated (Fig. 6*A* and Datasets S1 and S2). The 3D principal component analyses (3D-PCAs) verified that the differential transcriptomes of miR-dKO and WT EDs were indeed clustering separately (Fig. 6*B*). Using TargetScan (28), we identified 362 genes that could be targeted by the five miRNAs (miR-449a/b/c and -34b/c), including 202 up-regulated and 160 down-regulated (Dataset S3). Gene Ontology (GO) term analyses identified that these affected target genes were mostly involved in ciliogenesis, including axoneme assembly, microtubule bundle formation, cilium assembly, cilium organization, and other similar functions (Fig. 6*C*). Six dysregulated genes (Fig. 6*D*) known to be involved in ciliogenesis (*Cby1*, *Ccdc113*, *Dnah6*, *Sclt1*, *Tubb4b*, and *4931429l11Rik*) were chosen for validation of their expression levels by using qPCR (Fig. 6*E*). To further confirm the targeting relationship between miR-34b/c–miR-449a/b/c and the predicted target genes, luciferase reporter assays were performed on two significantly down-regulated genes in miR-dKO EDs, *Ccdc113* and *Dnah6*. *Ccdc113* is a component of centriolar satellites and plays a pivotal role in primary cilium

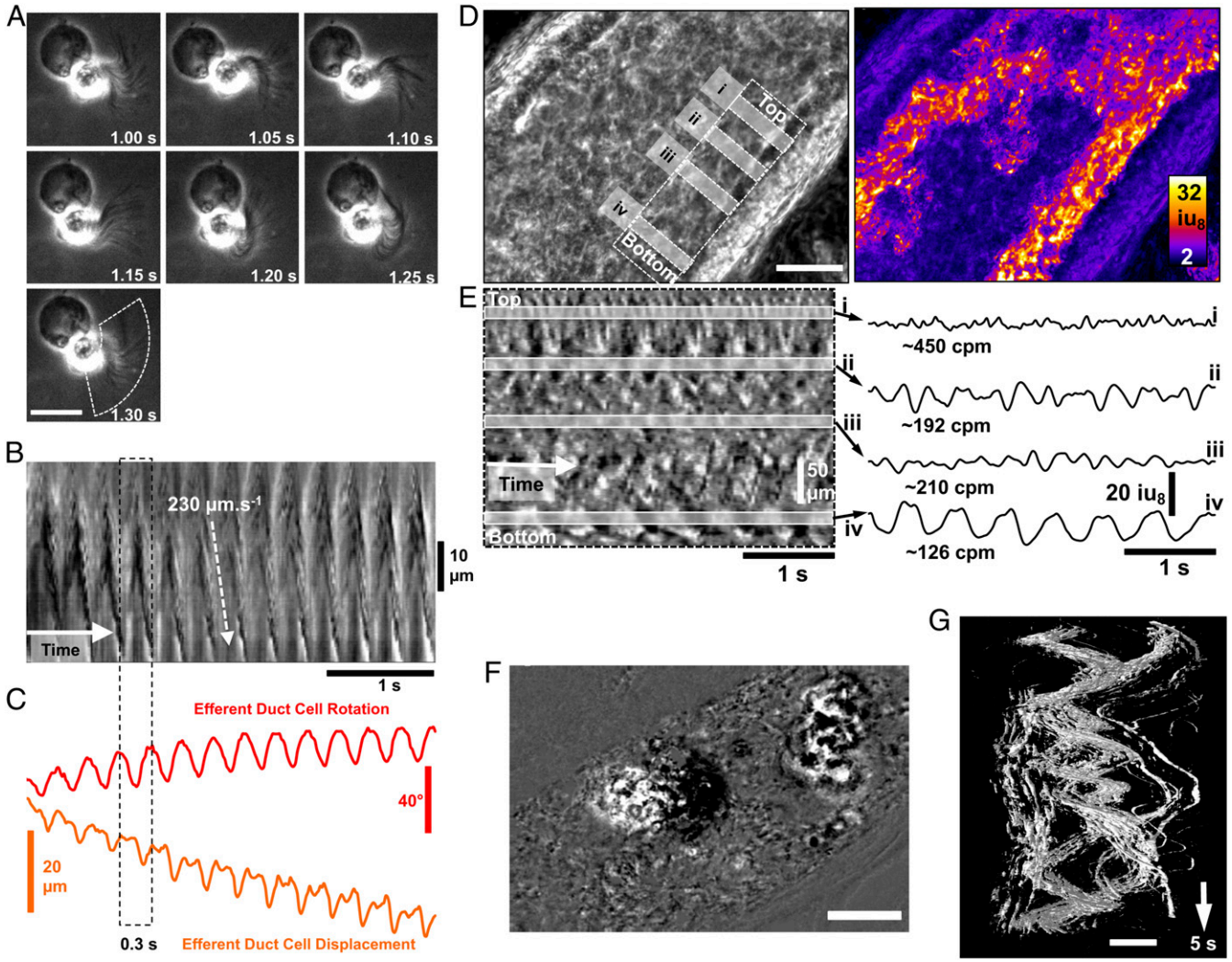

Fig. 4. Cilia beating patterns in isolated ciliated cells and intact EDs. (*A*) Image sequences showing the beating motion of cilia and the resulting rotation in a ciliated cell isolated from adult EDs. All frames are in the same scale. (Scale bar: 15 μm.) (*B*) An ST map (time in the *x* axis) showing changes in cilia opacity/translucency calculated perpendicularly to the overall arc of motion (see dashed region in *A*, *Bottom*). (*C*) Object displacement and rotation tracking of the isolated ciliated cell show the regularity of cilia motion and the propulsive effect on the cell. Efferent ductal cilia generate larger torque forces that rotate (±20° per beat) and displace the cell (±7–10 μm). (*D*) Image of the field of view (FOV) using power imaging of intact ED tube (*Left*) and SD of opacity/translucency demarcating those areas in which detectable cilia beating was observed (*Right*). (Scale bar: 100 μm.) (*E*, *Left*) An ST map (time in the *x* axis) taken from a region parallel to the ED wall showing distinct rhythmic frequencies (gray bars i–iv). (*E*, *Right*) Plotting the time courses of the changes in opacity/translucency reveals a wide variety of frequencies and amplitudes in adjacent regions [~450 cpm (i) to ~126 cpm (iv)]. (*F*) Differential image showing two clumps of materials (most likely cell clumps sloughed into the lumen during whole-mount preparation) within the EDs. (Scale bar: 100 μm.) (*G*) The 3D ST objects constructed from the two clumps of materials in *F*, showing the swirling motion applied to objects by the underlying movement of cilia. (Scale bar: 100 μm.)

formation (29), whereas *Dnah6* is known to interact with primary ciliary dyskinesia-related genes in humans and plays a role in multiciliogenesis (30). In the presence of the five miRNAs, the luciferase activities increased significantly (Fig. 6 *F*–*I*), suggesting that both *Ccdc113* and *Dnah6* are true targets of the five miRNAs. Taken together, our data suggest that the five miRNAs encoded by miR-34b/c–miR-449 clusters normally control the stability of multiple mRNAs involved in multiciliogenesis—e.g., *Ccdc113* and *Dnah6*—to ensure proper development of motile cilia in the efferent ductal epithelium.

Discussion

Motile cilia, which extend into the lumen from epithelial cells, are found only in a select number of vertebrate organs, but their importance to the health and survival of an organism cannot be ignored (1, 3). For example, the directional movement of mucus by ciliary beat over the surface of respiratory epithelium toward the oral cavity is essential for the prevention of chronic pulmonary infection and disease (31). Early studies of this highly coordinated beat of respiratory cilia, called the metachronal wave (32, 33), led to the adoption of a generalized dogma that all kinetic cilia move fluids over epithelial surfaces in a similar manner. The present studies conducted in male reproductive tissues found this idea to be incorrect. The cilial beat in EDs of the male produces a uniquely coordinated, whip-like motion, displaying a strong rotational force with each power stroke, confirming the hypothesis that ED cilia function is to mix the luminal contents (17, 27). This specialized beating pattern generates a centripetal force on the luminal fluid, as each ciliated cell can beat in a different direction, often opposing the direction of the ciliary beat in cells on the opposite side of the lumen. The beat results in a strong fluidic turbulence, which appears to aid in

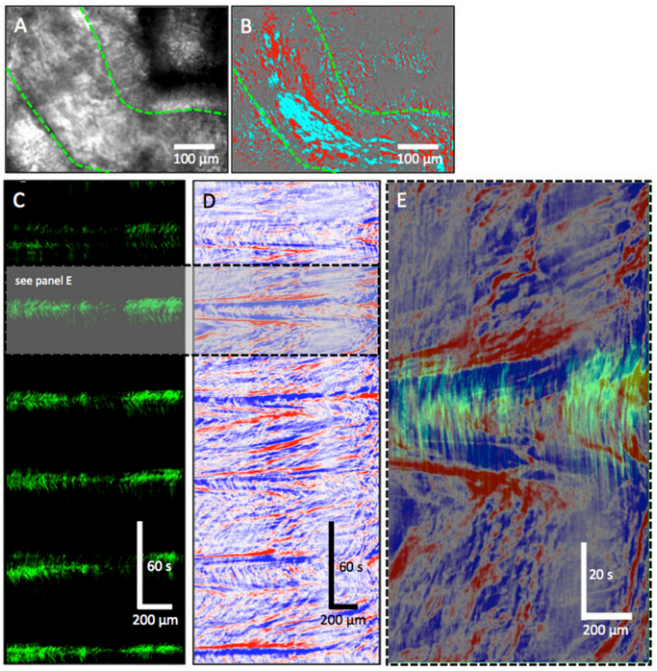

Fig. 5. Peristaltic contractions of the efferent ductal smooth muscle propel sperm to the epididymis. (*A*) Raw movie frame showing the efferent ductal wall (green dashed lines) and vessel lumen containing immotile sperm. (*B*) Differential imaging ($\Delta t \pm 5$ s) was used to remove static background to better delineate wall motion and sperm. (*C*) ST map of wall motion (upper green edge) showing regular peristaltic contractions that occurred approximately every minute (interval 58.5 ± 4.7 s; $o = 5$) and lasted ∼20 s. (*D*) ST map of the movement of contents (sperm) within the lumen of the ED. Peristaltic contractions of the ED smooth muscle propelled sperm rapidly at velocities of 100–300 $\mu m \cdot s^{-1}$. In between peristaltic contractions, sperm movement was variable and slow (10–70 $\mu m \cdot s^{-1}$). (*E*) Overlay of ST maps of a peristaltic contraction (see gray region in *C*; green) and content movement (see gray region in *D*; red/blue) showing the rapid propulsion of sperm during a peristaltic contraction.

the continual suspension of luminal spermatozoa. Testicular spermatozoa are released from the seminiferous epithelium and flushed by Sertoli cell secretions into the lumen of the rete testis, from which these immotile spermatozoa quickly transit through EDs to reach the caput epididymis (17). However, it is intriguing to consider how millions of immotile spermatozoa pass through these very narrow tubules without clogging, as their concentration is increased by nearly 25-fold due to fluid reabsorption by the nonciliated cells (34). The present study revealed that motile cilia of the EDs are essential for the passage of spermatozoa by ensuring their suspension, but not for their transport. Therefore, the ciliated cells function as individual agitators, and when this activity is lost, sperm aggregation occurs acutely, followed by eventual occlusion of the distal ED.

Is the ED ciliary beat the main force that propels spermatozoa toward the epididymis? Data presented here do not support this long-held presumption, because the fluidic turbulence generated by the highly variable ciliary beat pattern maintains spermatozoa in a swirling motion. If motile cilia were the only driving force for sperm transit through the EDs, their activity would fail, as sperm would continue to swirl within the lumen, without any significant movement toward the epididymis. By analyzing sperm movement within intact EDs ex vivo, it was clearly observed that peristaltic contractions of the smooth muscle cells served as the driving force to propel sperm forward. Spermatozoa move much more quickly back and forth in between contraction and relaxation, and the distances of forward movement by individual spermatozoa per contraction is far greater than those made by the swirling motion of the luminal fluid. This finding is consistent with prior observations suggesting that rhythmic smooth-muscle contractions represent a major component of sperm transport through EDs (25, 35, 36).

The data presented here demonstrate that motile cilia in EDs are essential for the passage of spermatozoa through the distal ED into the caput epididymis. The intratubal fluidic turbulence exists in every region of the EDs, and the swirling motion of the ciliary beat would presumably help reabsorption of fluid by (*i*) slowing down the flow rate (vertical vortices), thus allowing more contact time with microvilli on the nonciliated cell surface; and (*ii*) delaminating the fluid column, so that all parts of the column are exposed to the nonciliated cells. Therefore, in addition to the agitator function to prevent luminal occlusions, proper cilial beating may also be essential for an equilibrium in fluid reabsorption. The proximal EDs have larger diameters and fewer ciliated cells; this is in sharp contrast to the distal ED, which displays a smaller diameter and is populated by an increased number of ciliated cells. This structural feature may reflect fluid dynamic differences and advantages. For example, the sperm concentration in rete testis fluid is quite low but increases nearly 25-fold, as spermatozoa traverse the EDs and enter the initial segment of epididymis (34). The larger diameter of the proximal ED would decrease the flow rate and, thus, enhance initial fluid reabsorption. As fluid is reabsorbed, the increased sperm concentration results in elevated luminal viscosity, and at the same time, the ductules merge to form a much smaller single, common distal duct (25, 34). Therefore, the observed increase in the number of ciliated cells in the distal ED is a necessary adaptation to generate sufficient centripetal force to keep spermatozoa in suspension and to prevent clogging of the lumen.

Loss of motile cilia in the ED epithelium of miR-dKO and Foxj1-dcKO mice appears to have no significant impact on the nonciliated cells based on the following observations: (*i*) Our RNA-seq data revealed largely normal transcriptomic profiles for genes known to be expressed predominantly in nonciliated cells—*Esr1*, *Nhe3*, and *Pax8*—suggesting that functional compromise of nonciliated cells was very limited. (*ii*) Morphologically, the nonciliated cells appeared normal, although somewhat stretched in areas where the lumen was dilated. (*iii*) Histological examination of developing EDs showed that sperm agglutination occurred soon after the first batch of sperm transiting through the proximal segments of EDs, suggesting that ciliated cell defects are the primary cause of blockage because, otherwise, the sperm precipitation should have occurred at a later time. However, given the close interactions between the two cell types within the ED epithelium, an indirect effect of cilia loss on fluid reabsorption is likely. Disruption of the fluidic turbulence could alter the balance in ion transport across the epithelium and indirectly contribute to the agglutination of sperm. In the rooster, microlithiasis has been shown to be associated with sperm accumulation in EDs, as well as ductal occlusion leading to fluid build-up (37). Therefore, the mechanisms involved in the early onset of this lesion warrants further investigation. The accumulation of luminal fluid in the proximal region, as well as in the rete testis and seminiferous tubules, is similar to that reported for *Esr1* knockout and antiestrogen-treated mice, in which the primary lesion is the inhibition of nonciliated cell physiology of ion transport/exchange and water reabsorption (38, 39). Disruption of ESR1 activity does not produce ED obstruction, as spermatozoa in these animal models are found in the cauda epididymis (40); however, the ED luminal fluid cannot be reabsorbed and, thus, exceeds the transport capacity of the more narrow distal ED. In the miR-dKO and Foxj1-dcKO mice, the distal ED is blocked by large sperm aggregates, leading to the backup of luminal fluid, which appears to have exceeded the resorptive capacity of the nonciliated cells. Thus, in all

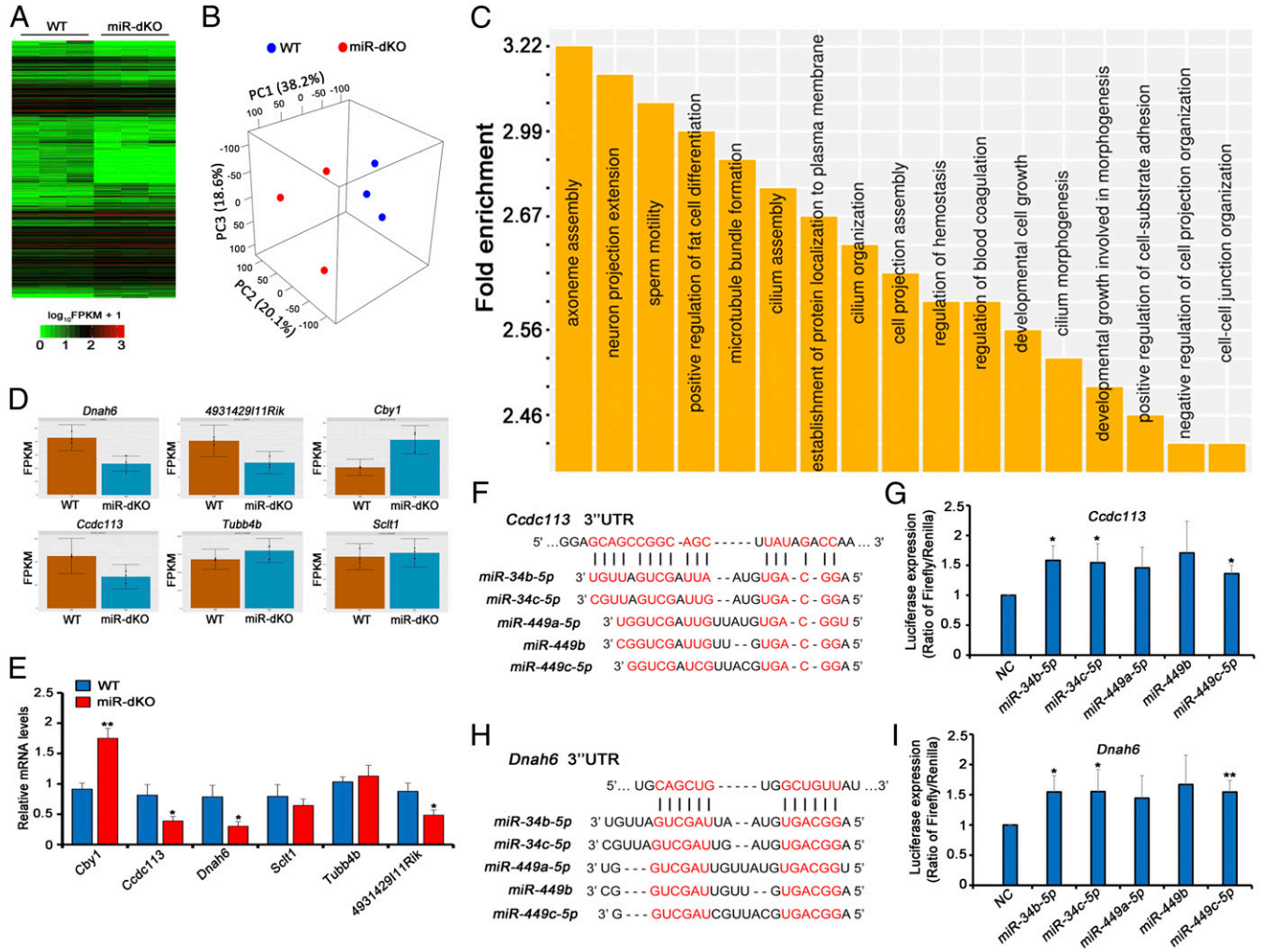

Fig. 6. miR-34b/c and -449a/b/c control multiciliogenesis in the EDs by regulating the expression of key genes involved in ciliogenesis. (*A*) A hierarchical clustering heatmap showing 7,002 significantly dysregulated mRNAs in miR-dKO EDs. (*B*) A 3D-PCA plot of the first three principal components (PCs) showing the clusters between WT and miR-dKO samples. The first three PCs account for 76.9% of the total variance, and samples of WT are distinctly separated from those of miR-dKO. (*C*) GO term enrichment analyses of significantly dysregulated mRNAs in miR-dKO EDs. Outputs (biological processes) are sorted and plotted against fold enrichment. (*D*) Levels of six representative, ciliogenesis-associated genes predicted to be targeted by the five miRNAs (miR-34b/c and -449a/b/c) based on RNA-seq data. (*E*) qPCR validation of the levels of the six target genes, as shown in *D*, in WT and miR-dKO EDs. *Gapdh* was used as the internal control for normalization. Data are presented as mean ± SEM (n = 3). $*P < 0.05$; $**P < 0.01$ (Student's *t* test). (*F* and *H*) Schematics showing two predicted miR-34/449-binding sites in the 3′ UTRs of *Ccdc113* (*F*) and *Dnah6* (*H*). (*G* and *I*) Luciferase-based reporter assays showing miR-34b/c–miR-449c–dependent stabilization of *Ccdc13* (*G*) and *Dnah6* (*I*) in HEK293 cells. Data are presented as mean ± SEM ($n = 3$). $*P < 0.05$; $**P < 0.01$ (Student's *t* test).

four animal models involving either nonciliated cell inhibition (*Esr1*KO and antiestrogen treatment) or motile cilia loss (miR-dKO and Foxj1-dcKO), the resulting testicular pathophysiology is the same: fluid accretion.

Given such important functions for motile cilia in the EDs, any disturbance that compromises the ciliary beat could alter the balance between fluid reabsorption and secretion, leading to a complete or partial ED obstruction. Excessive reabsorption can cause occlusion, while inhibition of reabsorption leads to the dilution of epididymal spermatozoa (16). Both situations result in fluid accumulation and backflow of ED fluid into the rete testis and seminiferous tubules and over time can produce testicular atrophy. The luminal back pressure and its associated dilation can lead to chronic spermatogenic impairments characterized by either oligoasthenoteratozoospermia (OAT) or azoospermia, depending on the duration of back pressure.

Unfortunately, textbook descriptions of the human epididymis have often omitted the fact that coiled EDs occupy a major portion of the caput epididymis in men (8, 16, 41). Thus, numerous manuscripts referring to lesions in the head of the epididymis may have overlooked potential pathological changes in EDs—e.g., loss of motile cilia—and/or ED obstructions. Patients with ED obstructions would be misdiagnosed as "nonobstructive azoospermia" (NOA) or "Sertoli cell-only syndrome" based on testicular biopsy, although the primary defect may lie in ED epithelia. This hypothesis is supported by two case reports, showing that men with the so-called "immotile cilia syndrome" display azoospermia (42, 43). Therefore, future consideration of ED pathology is warranted to determine whether ED obstructions may account for a proportion of NOA and OAT patients in fertility clinics. The findings that male fertility can be regained even after long-term spermatogenic disruptions due to back pressure caused by ED obstructions and fluid retention have significant clinical implications, because in similar cases of ED obstructions in men, it may be possible to regain sperm production through a surgical procedure to relieve the accumulating fluid pressure.

In summary, results presented here demonstrate an agitating ciliary beat by the ED epithelium and provide a better understanding of how the ED motile cilia have adapted to produce luminal fluid turbulence, which prevents spermatozoa from clogging the EDs. This finding has a significant translational potential to clinical applications, because ED occlusions may represent a major cause of human male infertility. Moreover, it is of interest to investigate whether similar ciliary beat patterns exist in other multiciliated organs (e.g., brain and spinal column).

Materials and Methods

Animals. All animal work was performed following the protocol approved by the Institutional Animal Care and Use Committee of the University of Nevada, Reno. Mice were housed and maintained under specific pathogen-free conditions with a temperature- and humidity-controlled animal facility in the University of Nevada, Reno. The *miR-dKO* mouse line was generated as described (14). *Stra8-Cre*, *Foxj1-Cre*, and *Rosa26-mTmG*$^{Tg/Tg}$ mice were purchased from the JAX. Generation of the miR-449-loxp mice were described (13). All mice used in this study were back-crossed to the C57BL/6J for at least five generations.

Histology and Immunofluorescent Analysis. EDs were dissected under stereoscopic microscope and fixed in Bouin's solution overnight at 4 °C, followed by paraffin embedding. Paraffin sections (6 μm) were cut and stained with hematoxylin and eosin (H&E) for histological analyses after deparaffinization and rehydration. For immunohistochemical staining, the EDs were dissected and fixed with 4% paraformaldehyde in PBS overnight at 4 °C. The fixed samples were then processed through a graded series of sucrose solutions (from 5 to 20%), followed by embedding in (1:1) 20% sucrose and optimal cutting temperature compound (Tissue-Tek, catalog no. 4583). Cryosections (5 μm) were cut and then washed twice in PBS with 0.05% Tween 20. After blocking in PBSTB (0.1% Triton X-100 and 1% BSA in PBS) for 1 h at room temperature (RT), the slides were incubated with primary antibodies overnight at 4 °C. The primary antibodies used included anti–β-tubulin IV monoclonal antibody (tubb4; 1:20; catalog no. MU178-UC, BioGenex), anti–acetylated-α-tubulin (1:50; T6793; Sigma), and antidetyrosinated α-tubulin (1:500; catalog no. ab48398, Abcam). After washing three times with cold PBST (0.1% Triton X-100 in PBS), the slides were incubated with a secondary antibody (1:1,000; Alexa Fluor 488 goat anti-rabbit or Alexa Fluor 555 conjugate goat anti-mouse; catalog no. A-21422, Molecular Probes) at RT for 1 h. Slides were mounted with VECTASHIELD mounting medium with DAPI (catalog no. H-1200, Vector Laboratories). Images were taken with an epifluorescence microscope (Axioplan 2; Carl Zeiss).

In Situ Hybridization. In situ hybridization was performed by using a microRNA ISH Optimization Kit (Exiqon Inc.) following the instructions. Probe sequences are as follows: has-miR-34c-5p, DigN-GCAATCAGCTAACTACACTGCCT; has-miR-449a, DigN-ACCAGCTAACAATACACTGCCA; and control, DigN-GTGTAACACGTCTATACGCCGA. Blue color developed by Nitro-Blue-tetrazolium/5-bromo-4-chloro-3-indolyl-phosphate staining represents specific hybridization signals, and the nuclei were counterstained with Fast Red.

Diameter Measurement and Epithelial Cell Counting. H&E-stained paraffin sections of the proximal and distal EDs were used for the diameter measurement and epithelial cell counting. Only those round-shaped EDs were chosen for diameter measurement using Adobe Photoshop (Version 2017). A total of 100–200 individual cross-sections from 6 or 12 mice were measured. While the diameters of the EDs were measured, the number of ciliated and nonciliated cells in the proximal and distal EDs was counted, respectively. A total of 50–100 individual cross-sections from 10 mice were used for cell counting. The ratios of nonciliated to ciliated cells were calculated.

Transmission Electron Microscopy Analysis. TEM was performed as described with some modifications (44). Briefly, the EDs were fixed in 0.1 M cacodylate buffer (pH 7.4) containing 3% paraformaldehyde and 3% glutaraldehyde plus 0.2% picric acid for 2 h in 4 °C, then for 1 h at RT. Following washes with 0.1 M cacodylate buffer, the samples were postfixed with 1% OsO_4 for 1 h at RT. Then, the samples were dehydrated in sequentially ethanol solutions (30%, 50%, 70%, 90%, and 100%) and embedded in Eponate mixture (Electron Microscopy Sciences) for polymerization for ∼24 h at 60 °C. Ultrathin sections (60–70 nm) were cut with a diamond knife. The sections were stained with uranyl acetate and lead citrate and then photographed by using a transmission electron microscope (Phillips CM10) at 80 kV.

qPCR Analysis. Large and small RNAs were isolated from the EDs of WT and *miR-dKO* mice by using the mirVana kit (Life Technologies). For mRNA quantification, after reverse transcription, the cDNAs were diluted to 50 ng/μL, followed by qPCR analyses using FAST SYBR Green (Applied Biosystems). Each reaction contained 50 ng of cDNA and 1 μL of primer mix, in a total of 20-μL reactions. miRNA qPCR analyses were performed as described (14, 15). qPCR analyses were performed on 7900HT Fast Real Time PCR System (Applied Biosystems). U6 snRNA was used for miRNA qPCR data normalization. Data were analyzed by the Student *t* test. A statistically significant difference was defined as $P < 0.05$. The primer sequences are listed in *SI Appendix*, Table S1.

Whole-Mount EDs and Video Recording. The whole testis, EDs, and epididymis were dissected in HBSS solution (catalog no. SH30588; HyClone) under a dissection microscope (catalog no. SZX2-ILLT; Olympus). The connective tissues surrounding the EDs were carefully removed. The whole testis, EDs, and epididymis were washed in HBSS several times and then transferred to a microcoverglass (20 × 50 mm; VWR) and covered by another smaller one. The whole-mount slides were placed on a upright microscope with a warming plate set at 35 °C. Movies of cilia movement were captured by using a monochrome camera at 60 fps (catalog no. DMK21AF04; Imaging Source), which was operated by the Astro IIDC software (Version 4.09.02) and attached to a Zeiss Axioskop 2 microscope.

Imaging Analysis.

Isolated cells. Movies were imported into custom-written software (Volumetry G8d; G.W.H.), movement of isolated cells was stabilized, and their rotation was tracked. The behavior of cilia was summarized by averaging the change in intensity of cilia radially out from the cell body. As the overlap and contrast of cilia varied (as light and dark areas) during the beating cycle, the propagation of waves of activity could be detected (Fig. 4 *A*–*C* and Movies S1 and S2), and measurements of frequency, velocity, and number of beating sites could be calculated.

Intact EDs. Lower-power movies of intact efferent ducts showed the distribution and frequency of cilia beating and the effect on intraluminal contents. To determine the actively beating regions within the duct, an SD map of the changes in pixel intensity during the movie was constructed and color-coded. In some ducts, the frequency of beating could be determined from ST maps constructed along the duct wall (Fig. 4 *D*–*G*). To visualize and quantify the agitation of intraluminal contents created by the ciliated epithelium, the movie was differentiated ($\Delta t = 5$ s), and moving objects were thresholded to allow tracking and 3D reconstruction at an ST cube (Fig. 4*G* and Movie S3).

Efferent duct wall motion. Due to the high background and depth of focus, edge-detection methods were unreliable to quantify wall motion and content movement in movies of efferent ducts. Instead, the movie was differentiated ($\Delta t \pm 5$ s), which removed static background and allowed visualization of moving objects with a ±5-s time window. The positive (future) and negative (past) changes were thresholded by using red and cyan, respectively. This created two distinct motion signatures: (*i*) the duct wall as a slow, structurally stable differential signature; and (*ii*) intraluminal volume as a fast moving, constantly changing differential signature. A line region of interest (ROI) was drawn over the edges of the efferent duct wall, and the sum of thresholded differential duct wall movements was averaged perpendicular to that line—creating an ST map of wall movement. A line ROI was also drawn in the middle of the vessel, and ST maps were created to show luminal content (sperm) propagation. Overlaying both maps showed the relationship between wall motion and flow. Intraluminal content velocities were calculated by using linear regression along the leading edge of the differential motion signature in STMaps, where horizontal distance of the line = spatial distance and vertical distance = time.

RNA-Seq and Data Analysis. Large RNAs were isolated from WT and miR-dKO EDs by using the AquaRNA RNA Purification Kit (catalog no. 5001MT; MoBiTec, Inc.). The mRNA and sncRNA libraries were constructed by using the TruSeq Stranded Total RNA Library Prep Kit (catalog no. RS-122-2201; IlBumina). Sequencing was conducted by using Hi-Seq 4000 sequencers with PE75 at BGI Bioscience. The FASTX-Toolkit was used to remove adaptor sequences and low-quality reads from the sequencing data. To identify all of the transcripts, we used Tophat2 and Cufflinks to assemble the sequencing reads based on the UCSC MM9 mouse genome (45). The differential expression analysis was performed by Cuffdiff (45). The global statistics and quality controls are presented in *SI Appendix*, Fig. S6.

In Silico miRNA Target Prediction. The 3′ UTR sequences for each RNA isoform was extracted by in-house R script based on Splice R analyses. RNAhybrid was

used to perform the binding analyses between the 3′ UTR sequence and the miRNA sequence (46) (RNAhybrid –c –s 3utr_human –p 0.1 -f 2,7). The output results were imported into R as data frame for downstream analyses.

Luciferase Reporter Assay. For luciferase reporter assays, the 3′ UTRs of *Ccdc113* and *Dnah6* were amplified from mouse cDNA by PCR using GoTaq Green Master Mix (catalog no. M7123; Promega). The PCR products were inserted into psiCHECK-2 vector at XhoI and NotI restriction sites by using T4 DNA ligase (catalog no. M0202S; NEB), which are downstream of the *Renilla* luciferase-coding sequence. HEK293 cells were cotransfected with 5 pmol of miRNA mimics or negative control (GE Dharmacon) and 150 ng of psiCHECK-2 containing *Ccdc113* or *Dnah6* 3′ UTRs by using Lipofectamine 2000 (catalog no. 11668; Invitrogen) in a 240-well cell culture plate (catalog no. 3524; Corning). After 24 h, cells were lysed and assayed with the Dual Luciferase Assay Kit (catalog no. E1910; Promega), according to the instructions of the manufacturer. *Renilla* luciferase signals were normalized to *Firefly* luciferase signals to correct for transfection efficiency. The primers were synthesized by IDT, and the sequences are listed in *SI Appendix*, Table S1.

Statistical Analysis. All data were presented as mean ± SEM, and statistical differences between datasets were assessed by one-way ANOVA or the Student *t* test by using the SPSS16.0 software. $P < 0.05$ was considered as significant differences, and $P < 0.01$ was considered as highly significant differences.

Availability of Data and Materials. The RNA-seq data have been deposited into the National Center for Biotechnology Information Sequence Read Achieve database (47) (accession no. PRJNA454757).

ACKNOWLEDGMENTS. We thank Dr. Michael Kessel (Max Planck Institut für Biophysikalische Chemie) for providing us with the miR-449 loxp mice. This work was supported by NIH Grants HD071736 and HD085506 (to W.Y.); Templeton Foundation Grant PID 50183 (to W.Y.); National Natural Science Foundation of China Grants 81471497 (to C.X.) and 81671509 (to J.W.); Shanghai Natural Science Foundation Grant 12JC1405500 (to C.X.); and Shanghai Municipal Commission of Health and Family Planning Foundation Grant 201540270 (to J.W.). RNA-seq was conducted in the Single Cell Genomics Core of the University of Nevada, Reno, School of Medicine, which was supported in part by NIH Centers of Biomedical Research Excellence Grant 1P30GM110767.

1. Satir P, Christensen ST (2008) Structure and function of mammalian cilia. *Histochem Cell Biol* 129:687–693.
2. Braun DA, Hildebrandt F (2016) Ciliopathies. *Cold Spring Harb Perspect Biol* 9: a028191.
3. Afzelius BA (2004) Cilia-related diseases. *J Pathol* 204:470–477.
4. Wong LB, Miller IF, Yeates DB (1993) Nature of the mammalian ciliary metachronal wave. *J Appl Physiol (1985)* 75:458–467.
5. O'Callaghan C, Sikand K, Chilvers MA (2012) Analysis of ependymal ciliary beat pattern and beat frequency using high speed imaging: Comparison with the photomultiplier and photodiode methods. *Cilia* 1:8.
6. Li S, et al. (2017) Estrogen receptor α is required for oviductal transport of embryos. *FASEB J* 31:1595–1607.
7. Hess RA (2002) The efferent ductules: Structure and functions. *The Epididymis: From Molecules to Clinical Practice*, eds Robaire B, Hinton B (Kluwer Academic/Plenum, New York), pp 49–80.
8. Hess RA (2018) Efferent ductules: Structure and function. *Encyclopedia of Reproduction*, ed Skinner MK (Academic/Elsevier, San Diego), 2nd Ed, Vol 1, pp 270–278.
9. Clulow J, Jones RC, Hansen LA, Man SY (1998) Fluid and electrolyte reabsorption in the ductuli efferentes testis. *J Reprod Fertil Suppl* 53:1–14.
10. Francavilla S, Moscardelli S, Bruno B, Barcellona PS, De Martino C (1986) The postnatal maturation of efferent tubules in the rat: A light and electron microscopy study. *J Embryol Exp Morphol* 96:51–63.
11. Ross MH, Pawlina W (2016) *Histology: A Text and Atlas* (Wolters Kluwer Health, Philadelphia), 7th Ed.
12. Young B, Heath JW (2000) *Wheater's Functional Histology: A Text and Colour Atlas* (Churchill Livingstone, London), 4th Ed.
13. Song R, et al. (2014) miR-34/449 miRNAs are required for motile ciliogenesis by repressing cp110. *Nature* 510:115–120.
14. Wu J, et al. (2014) Two miRNA clusters, miR-34b/c and miR-449, are essential for normal brain development, motile ciliogenesis, and spermatogenesis. *Proc Natl Acad Sci USA* 111:E2851–E2857.
15. Yuan S, et al. (2015) mir-34b/c and mir-449a/b/c are required for spermatogenesis, but not for the first cleavage division in mice. *Biol Open* 4:212–223.
16. Hess RA (2014) Disruption of estrogen receptor signaling and similar pathways in the efferent ductules and initial segment of the epididymis. *Spermatogenesis* 4:e979103.
17. Hess RA (2015) Small tubules, surprising discoveries: From efferent ductules in the turkey to the discovery that estrogen receptor alpha is essential for fertility in the male. *Anim Reprod* 12:7–23.
18. Bao J, Ma HY, Schuster A, Lin YM, Yan W (2013) Incomplete cre-mediated excision leads to phenotypic differences between Stra8-iCre; Mov10l1(lox/lox) and Stra8-iCre; Mov10l1(lox/Δ) mice. *Genesis* 51:481–490.
19. Hess RA (2018) Endocrinology and pathology of rete testis and efferent ductules. *Encyclopedia of Reproduction*, ed Skinner MK (Academic/Elsevier, San Diego), 2nd Ed, Vol 1, pp 279–285.
20. Joseph A, Shur BD, Ko C, Chambon P, Hess RA (2010) Epididymal hypo-osmolality induces abnormal sperm morphology and function in the estrogen receptor alpha knockout mouse. *Biol Reprod* 82:958–967.
21. Zhang Y, et al. (2007) A transgenic FOXJ1-Cre system for gene inactivation in ciliated epithelial cells. *Am J Respir Cell Mol Biol* 36:515–519.
22. Danielian PS, Hess RA, Lees JA (2016) E2f4 and E2f5 are essential for the development of the male reproductive system. *Cell Cycle* 15:250–260.
23. Smith G (1962) The effects of ligation of the vasa efferentia and vasectomy on testicular function in the adult rat. *J Endocrinol* 23:285–299.
24. Afzelius BA (2004) Cilia-related diseases. *J Pathol* 204:470–477.
25. Talo A (1981) In-vitro spontaneous electrical activity of rat efferent ductules. *J Reprod Fertil* 63:17–20.
26. Guttroff RF, Cooke PS, Hess RA (1992) Blind-ending tubules and branching patterns of the rat ductuli efferentes. *Anat Rec* 232:423–431.
27. Ilio KY, Hess RA (1994) Structure and function of the ductuli efferentes: A review. *Microsc Res Tech* 29:432–467.
28. Agarwal V, Bell GW, Nam JW, Bartel DP (2015) Predicting effective microRNA target sites in mammalian mRNAs. *eLife* 4:e05005.
29. Firat-Karalar EN, Sante J, Elliott S, Stearns T (2014) Proteomic analysis of mammalian sperm cells identifies new components of the centrosome. *J Cell Sci* 127:4128–4133.
30. Li Y, et al. (2016) DNAH6 and its interactions with PCD genes in heterotaxy and primary ciliary dyskinesia. *PLoS Genet* 12:e1005821.
31. Knowles MR, Zariwala M, Leigh M (2016) Primary ciliary dyskinesia. *Clin Chest Med* 37: 449–461.
32. Elgeti J, Gompper G (2013) Emergence of metachronal waves in cilia arrays. *Proc Natl Acad Sci USA* 110:4470–4475.
33. Gheber L, Priel Z (1990) On metachronism in ciliary systems: A model describing the dependence of the metachronal wave properties on the intrinsic ciliary parameters. *Cell Motil Cytoskeleton* 16:167–181.
34. Clulow J, Jones RC, Hansen LA (1994) Micropuncture and cannulation studies of fluid composition and transport in the ductuli efferentes testis of the rat: Comparisons with the homologous metanephric proximal tubule. *Exp Physiol* 79:915–928.
35. MacMillan EW, Harrison RG (1955) The rate of passage of radiopaque medium along the ductus epididymidis of the rat. *Proc Soc Study Fertil* 7:35–40.
36. Winet H (1980) On the mechanism for flow in the efferent ducts. *J Androl* 1:303–311.
37. Nistal M, García-Cabezas MA, Regadera J, Castillo MC (2004) Microlithiasis of the epididymis and the rete testis. *Am J Surg Pathol* 28:514–522.
38. Hess RA, et al. (1997) A role for oestrogens in the male reproductive system. *Nature* 390:509–512.
39. Hess RA, Cooke PS (2018) Estrogen in the male: A historical perspective. *Biol Reprod* 99:27–44.
40. Cho HW, et al. (2003) The antiestrogen ICI 182,780 induces early effects on the adult male mouse reproductive tract and long-term decreased fertility without testicular atrophy. *Reprod Biol Endocrinol* 1:57.
41. Yeung CH, Cooper TG, Bergmann M, Schulze H (1991) Organization of tubules in the human caput epididymidis and the ultrastructure of their epithelia. *Am J Anat* 191: 261–279.
42. Bashi S, Khan MA, Guirjis A, Joharjy IA, Abid MA (1988) Immotile-cilia syndrome with azoospermia: A case report and review of the literature. *Br J Dis Chest* 82:194–196.
43. Dixit R, Dixit K, Jindal S, Shah KV (2009) An unusual presentation of immotile-cilia syndrome with azoospermia: Case report and literature review. *Lung India* 26: 142–145.
44. Yuan S, Zheng H, Zheng Z, Yan W (2013) Proteomic analyses reveal a role of cytoplasmic droplets as an energy source during epididymal sperm maturation. *PLoS One* 8:e77466.
45. Trapnell C, et al. (2012) Differential gene and transcript expression analysis of RNA-seq experiments with TopHat and Cufflinks. *Nat Protoc* 7:562–578.
46. Krüger J, Rehmsmeier M (2006) RNAhybrid: microRNA target prediction easy, fast and flexible. *Nucleic Acids Res* 34:W451–W454.
47. Yan W (2018) Data from "Mus musculus strain:C57 (house mouse)." Sequence Read Achieve. Available at https://www.ncbi.nlm.nih.gov/bioproject/?term=PRJNA454757. Deposited May 3, 2018.